Time-Dependent Mechanical Behavior of Chiral Cosserat Materials

Cheng-Wei Mai[1], Wan-Chun Lo[1], Yun-Che Wang[1,*] and Yasothorn Sapsathiarn[2]

[1] Department of Civil Engineering, National Cheng Kung University, Tainan, TAIWAN
[3] Department of Civil and Environmental Engineering, Faculty of Engineering, Mahidol University, Nakhon Pathom, THAILAND
**Corresponding author; E-mail address: yunche@ncku.edu.tw*

Abstract

Chiral Cosserat materials possess extra internal degrees of freedom, as opposed to those assumed in classical elasticity. Hence, nine material parameters are required to describe the isotropic and homogeneous Cosserat materials with chirality. Chirality indicates the loss of centrosymmetric assumptions in constitutive relationships. In addition, mass density and micro inertia are required for modeling dynamic behavior. Classical isotropic and homogeneous linear elastic materials only require two independent material parameters. Through finite element numerical studies, it is shown that the chiral Cosserat materials can exhibit Poisson's ratio greater than 0.5, or smaller than -1. These ranges are not allowed in classical elastic material due to the violation of the positive definiteness of strain energy density. Furthermore, the time-dependent deformation mode couplings, such as tension-induced bending or torsion, are investigated. The couplings may serve as a sensing capability in such materials. Our study on the non-classical material systems may expand the material design and selection space in engineering applications, which are not achievable in traditional construction materials.

Keywords: Time-Dependent Mechanical Behavior, Chiral Cosserat Material, Viscoelasticity, Finite Element Analysis

1. Introduction

Materials described by the theory of elasticity only allow translational degrees of freedom at a given material point. The theory of elasticity is successful in describing materials without microstructure. For materials with microstructure, such as lattice materials, theories for generalized continua are required, such as the Cosserat theories. When the Cosserat materials do not possess centrosymmetry, the chiral Cosserat material model is required [1, 2]. When material parameters are time-dependent, as described in the theory of linear viscoelasticity, one needs to use the Boltzmann superposition principle to modify the constitutive relations [3]. When material properties are time-independent, it has been shown in Ref. [2] that chiral Cosserat materials can exhibit physical Poisson's ratio beyond the classical elasticity range, i.e. $-1 < \nu < 0.5$, stated in elasticity to ensure strain energy density being positive definite. Negative Poisson's ratio is related to negative bulk modulus and extreme viscoelastic damping [4,5].

The aforementioned theories are based on the concept that the materials are of continuum. One can also construct discrete materials with microstructure, and calculate the effective properties to exhibit the Cosserat [6,7] and chiral Cosserat [8] phenomena through homogenization via finite element calculations. In classical elasticity, when Poisson's ratio is outside the pointwise stability range, elastic moduli can become negative. Negative-stiffness composites are realizable and have shown extreme effective viscoelastic moduli [9,10] and damping [11]. Furthermore, negative-stiffness inclusions can enhance effective coupled-field properties, such as piezoelectric and pyroelectric coefficients [12,13,14].

In this work, we adopt the analytical and finite element methods to calculate the physical Poisson's ratio of the chiral Cosserat material in the framework of elasticity and linear viscoelasticity. We show that the physical Poisson's ratio can go beyond the classical elasticity range without violating pointwise stability conditions. These findings expand the parameter space for real-life engineering design.

2. Theoretical and Numerical Aspects

The constitutive relations for stress components σ_{ij} of the chiral Cosserat solids can be calculated from elastic strain ε_{ij}, as follows.

$$\begin{aligned}\sigma_{ij} &= \lambda\varepsilon_{mm}\delta_{ij} + 2G\varepsilon_{ij} \\ &\quad + \kappa e_{ijm}\left(r_m - \phi_m\right) \\ &\quad + C_1\phi_{m,m}\delta_{ij} + C_2\phi_{i,j} + C_3\phi_{j,i}\end{aligned} \tag{1}$$

The required material parameters to calculate the stress tensor are λ, G, κ, C_1, C_2, and C_3. To calculate the couple stress components, the following equation is adopted with three additional material parameters: α, β, γ. Hence, there are nine

material parameters for the chiral Cosserat materials. If the material is of the Cosserat type, the three parameters, C's, are neglected. The couple stress components are obtained from the following equation.

$$\begin{aligned} m_{ij} &= \alpha\phi_{m,m}\delta_{ij} + \beta\phi_{i,j} + \gamma\phi_{j,i} \\ &+ C_1\varepsilon_{m,m}\delta_{ij} + (C_2 + C_3)\varepsilon_{i,j} \\ &+ (C_3 - C_2)e_{ijm}(r_m - \phi_m) \end{aligned} \quad (2)$$

In the above equations, the macroscopic rotation vector of a stress element is

$$r_m = \frac{1}{2}e_{mij}u_{j,i} \quad (3)$$

Here e_{mij} is the permutation tensor, and u_j is the displacement vector. A common in the subscript indicates a partial differentiation with respect to a space coordinate. The physical shear modulus is related to the material parameters used in Eq. (1), as follows.

$$G = \mu + \frac{\kappa}{2} \quad (4)$$

When the material satisfies the assumptions of the classical elasticity, there is no difference between physical shear modulus and mathematical shear modulus, i.e. G = μ. The physical Poisson's ratio is defined as follows when the specimen is a right cylinder.

$$\nu = -\frac{\varepsilon_{rr}}{\varepsilon_{zz}} \quad (5)$$

The denominator is the applied longitudinal strain, and the numerator is the lateral strain, calculated from the radial displacement u_r.

$$\varepsilon_{rr} = \frac{\partial u_r}{\partial r} \quad (6)$$

The above equations only consider the material's elasticity responses with additional micro-rotation degrees of freedom. When linear viscoelasticity is considered, we only assume the shear modulus is time-dependent and can be modeled as a standard linear solid. Although other material parameters may also exhibit viscoelastic behavior, we limit ourselves, in this work, to only the shear modulus being viscoelastic as a demonstration of viscoelastic effects.

3. Results and discussion

The static physical Poisson's ratio, as a function of radius R_0, of the right cylinder for $C_1 = 10^4$, $C_2 = 5 \times 10^4$ and $C_3 = 10^5$ is shown in Figure 1. These results are obtained by analytically solving Eq. (5) when the right cylinder is under static elasticity assumptions with suitable boundary conditions. It can be seen that the smallest Poisson's ratio is about -3.3. When one judicially choose a parameter set for the mathematical material parameters used in Eq. (1) and (2), a physical Poisson's ratio can be obtained, and its value can go beyond the classical elasticity range, i.e. less than -1 or greater than 0.5.

Figure 2 shows our analytical results for static, physical Poisson's ratio to be as large as 1.9. In the legend of Figure 2, muC is equal to G. Physical Poisson's ratio is a function of cylinder radius R_0 is due to the effects of the intrinsic length scale of the chiral Cosserat material model. For the classical Cosseat material, its physical Poisson's ratio stays inside the classical elasticity range. The data shown in Figures 1 and 2 are analytical results and serve as a reference to sompare with the subsequent viscoelastic cases.

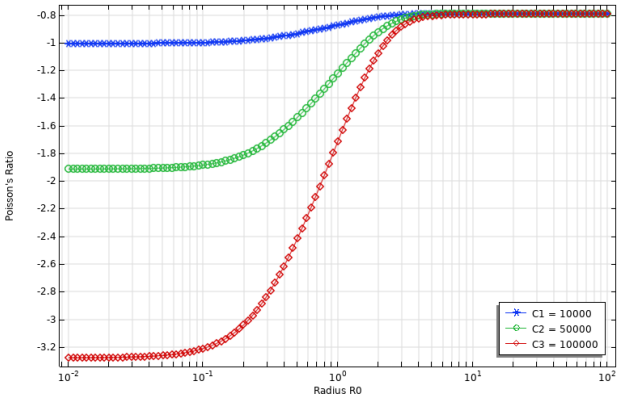

Fig. 1 Physical Poisson's rato of a cylinder with various radius R_0, in units of mm, for different C_1, C_2 and C_3 values

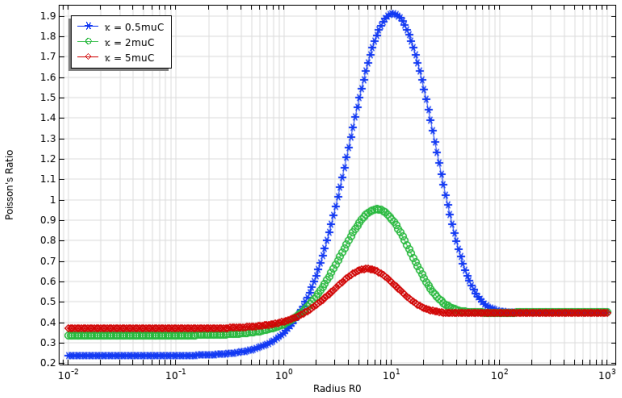

Fig. 2 Physical Poisson's rato of a cylinder with various radius R_0, in units of mm, for three different **K** values

When the linear viscoelasticity is considered, we choose the mathematical material parameters so that the static Poisson's ratio equals to **V** = 0.45 or 0.52. Figure 3 shows the lateral strain and applied axial strain when **V** = 0.45. Note the minus lateral strain is plotted. To avoid numerical difficulties at time near zero, the applied axial strain near time zero is smoothed so that the first derivative of the applied strain at time zero is continuous. The ratio of the minus lateral strain to the applied axial strain, i.e.

the Poisson's ratio, is shown in Figure 4. It can be seen that with our chosen material parameters, the fully relaxed Poisson's ratio in the viscoelastic study approaches the static value, i.e. 0.45.

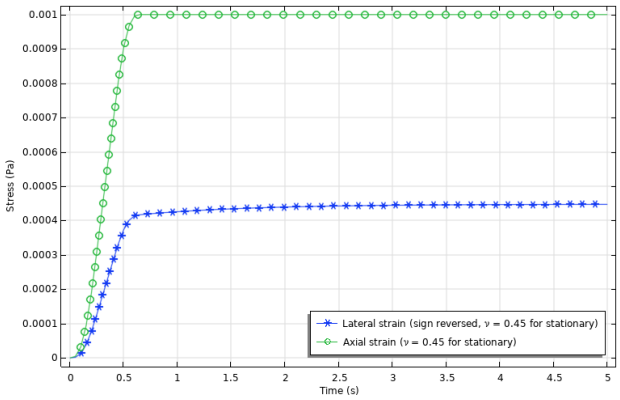

Fig. 3 The magnitude of lateral strain versus applied axial strain for static Poisson's ratio **V** = 0.45

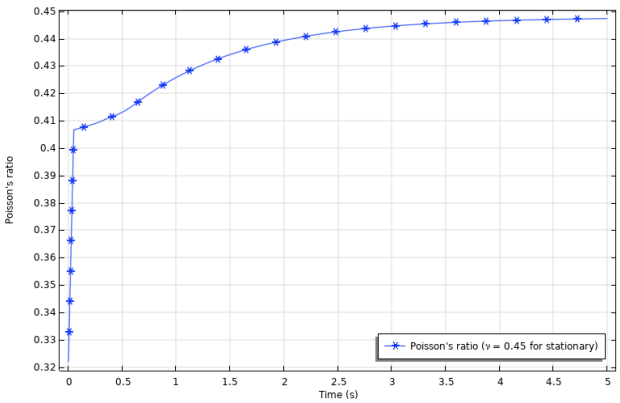

Fig. 4 Time-dependent Poisson's ratio when the static Poisson's ratio is assumed to be **V** = 0.45

Figure 5 shows the lateral strain and applied strain when **V** = 0.52. The maximum applied strain is set to be 0.001 to avoid geometric nonlinearity. After the ramp part of the applied strain, the applied strain remains constant to show the stress relaxation behavior of the material. The lateral response of the chiral Cosserat is quite different from that when **V** = 0.45. It is noted that when **V** = 0.52, the mathematical material parameters in Eq. (1) and Eq. (2) are so chosen that the static, physical Poisson's ratio is outside the classical elasticity range. Therefore, the non-monotonic behavior in the lateral strain is due to its physical Poisson's ratio greater than 0.5. Figure 6 shows the calculated Poisson's from the applied and lateral strain shown in Figure 5.

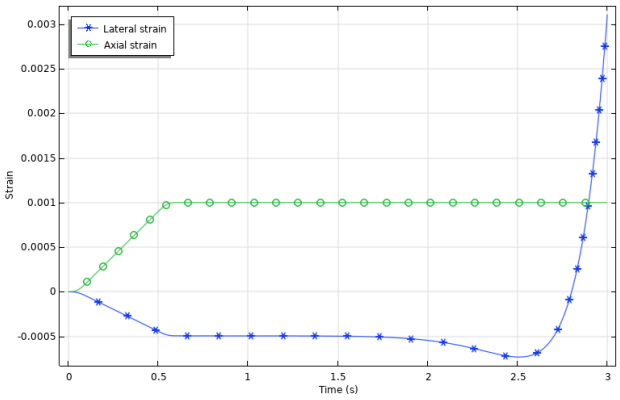

Fig. 5 The magnitude of lateral strain versus applied axial strain for static Poisson's ratio **V** = 0.52

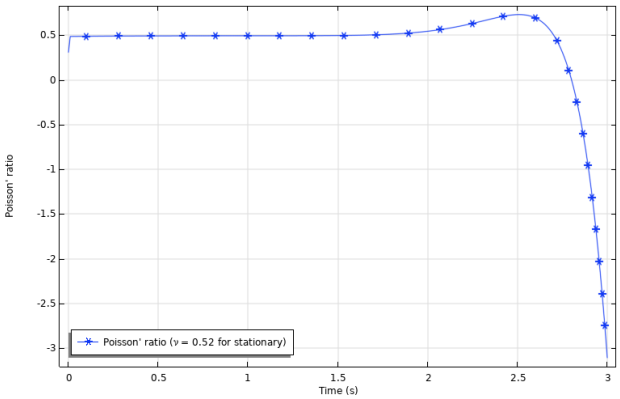

Fig. 6 Time-dependent Poisson's ratio when the static Poisson's ratio is assumed to be **V** = 0.52

From Figures 3, 4, 5 and 6, one can directly compare the viscoelastic responses of the chiral Cosserat materials with the two different static Poisson's ratio, i.e. **V** = 0.45 or 0.52. When **V** = 0.45, the material behaves as the conventional viscoelastic material, i.e., the Poisson's ratio is a monotonic function in time. However, when **V** = 0.52, the chiral material exhibits a static Poisson's ratio beyond classical elasticity range, and its viscoelastic Poisson's ratio is a non-monotonic function in time. When time is less than about 2.5 in Figure 6, the Poisson's ratio is monotonically increasing. However, when time is greater than 2.5, it drastically decreases.

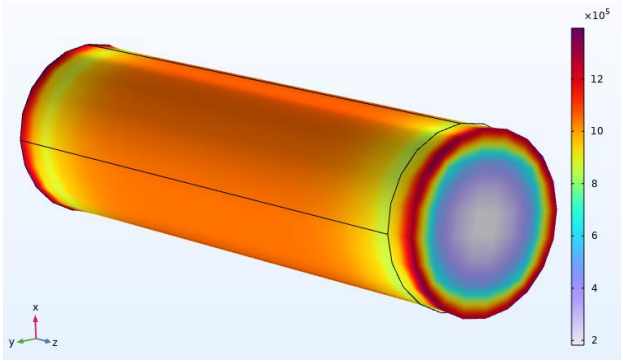

Fig. 7 von Mises stress when t = 5 s and static Poisson's ratio **ν** = 0.45. The left end of the cylinder is fixed, and the applied axial strain is on its right end.

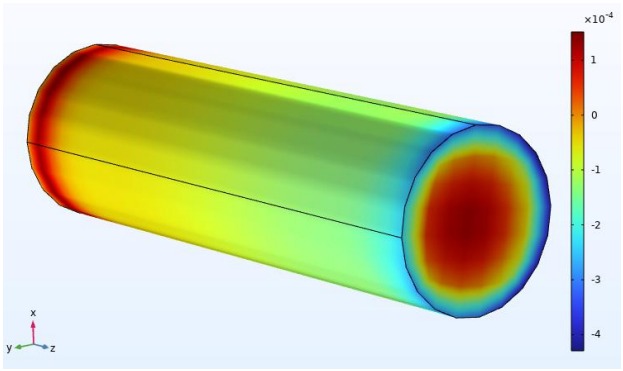

Fig. 8 Magnitude of micro-rotation vector when t = 5 s and static Poisson's ratio **ν** = 0.45.

Non-monotonicity in viscoelastic Poisson's ratio has been demonstrated by incorporating more than two phases with different Poisson's ratios with various relaxation time constants. Hence, under uniaxial straining, overall Poisson's ratio will change in accordance with each phase's Poisson's ratio and relaxation time to achieve non-monotonic behavior in the time domain. Here, we show non-monotonic Poisson's ratio in the chiral Cosserat material without resorting to multiple phases and multiple time constants.

When static Poisson's ratio **ν** = 0.45, the von Mises stress distribution and deformed geometry of the right cylinder is shown in Figure 7. Its color bar is in units of Pa. The corresponding micro-rotation vector magnitude in units of radian is shown in Figure 8. It can be seen that the St. Venant effects near the fixed-end boundary, i.e. the left end, cause stress magnitudes to increase for the **ν** = 0.45 case. These phenomena are different from the results for **ν** = 0.52 case, as shown below.

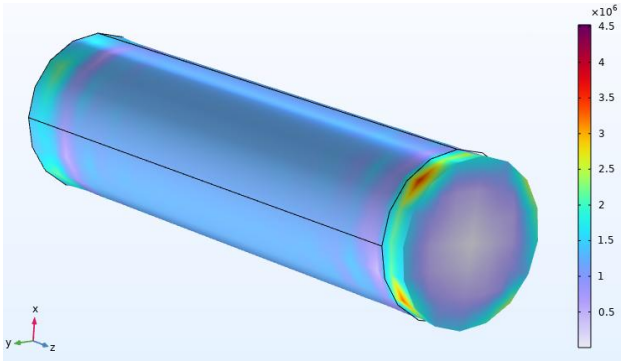

Fig. 9 von Mises stress when t = 0.6 s and static Poisson's ratio **ν** = 0.52. The left end of the cylinder is fixed, and the applied axial strain is on its right end.

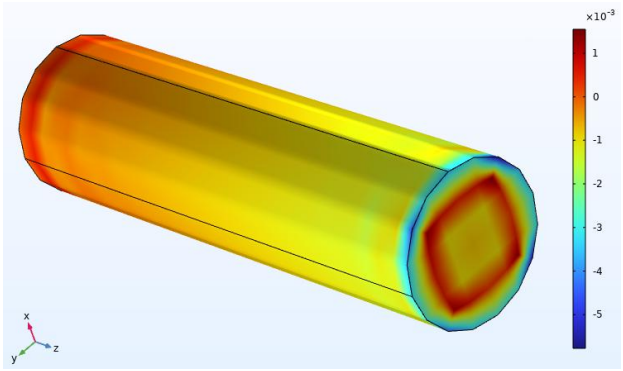

Fig. 10 Magnitude of micro-rotation vector when t = 0.6 s and static Poisson's ratio **ν** = 0.52.

When static Poisson's ratio **ν** = 0.52, the von Mises stress distribution and deformed geoemtry of the right cylinder is shown in Figure 9. Its color bar is in units of Pa. The corresponding micro-rotation vector magnitude in units of radian is shown in Figure 10.

From Figures 7, 8 , 9 and 10, one can directly compare the effects of static Poisson's ratio, i.e. **ν** = 0.45 or 0.52, on the distributions of field variables. Although the four figures are at different snapshots in the time domain, all of them are so chosen that the applied strain is outside the ramp. For the von Mises stress, shown in Figures 7 and 9, its magnitude is larger when **ν** = 0.45, while it becomes quite small when **ν** = 0.52, even though the color bars do not have the same scale. Both cases show the von Mises stress exhibits concentric distribution in the radial direction. However, the magnitude of micro-rotation is greatly increased in the **ν** = 0.52 case to compensate for the smaller deformation energy due to contributions from the Cauchy-type stress. In addition, the distribution of the micro-rotation is in a square shape for the **ν** = 0.52 case, while it is in a circular shape for the **ν** = 0.45 case.

4. Conclusions

The viscoelastic responses of the chiral Cosserat materials are numerically analyzed via the finite element method for their physical Poisson's ratio. Analytical results of the static physical Poisson's ratio of the chiral Cosserat materials are analytically obtained to show that the classical elasticity range, $-1 < \mathbf{V} < 0.5$, can be broken, while the strain energy positive definiteness can still be satisfied. When the shear modulus is assumed to be viscoelastic, we found viscoelastic Poisson's ratio may be non-monotonic in time when under the stress relaxation test if its static Poisson's ratio is beyond 0.5. If not, the viscoelastic Poisson's ratio satisfies monotonicity. These findings may expand the search of material parameter space for real-life engineering design, as well as the understanding of material behavior outside the conventional range.

Acknowledgments

This research is supported, in part, by the Yushan Fellow Program (Project No. MOE-113-YSFEE-0005-001-P1) by the Ministry of Education (MOE), Taiwan, and Taiwan National Science and Technology Council (NSTC 112-2221-E-006-049-MY3) with the New South Policy.

References

[1] Lakes, R.S. & Benedict, R.L. (1982). Noncentrosymmetry in micropolar elasticity. International Journal of Engineering Science, 20, pp. 1161-1167.

[2] Lakes, R.S., Huey, B. & Goyal, K. (2022). Extended Poisson's ratio range in chiral isotropic elastic materials, Physica Status Solidi b 259, 2200336.

[3] Eringen, A.C. (1967). Linear theory of micropolar viscoelasticity, International Journal of Engineering Science, 5, pp. 191-204.

[4] Wang, Y. C. & Lakes, R. S. (2005). Composites with inclusions of negative bulk modulus: extreme damping and negative Poisson's ratio. Journal of Composite Materials, 39(18), 1645-1657.

[5] Lakes, R. & Wojciechowski, K. W. (2008). Negative compressibility, negative Poisson's ratio, and stability. Physica Status Solidi (b), 245(3), 545-551.

[6] Wang, Y. C., Shen, M. W. & Liao, S. M. (2017). Microstructural effects on the Poisson's ratio of star-shaped two-dimensional systems. Physica Status Solidi (b), 254(12), 1700024.

[7] Wang, Y. C. (2019). Negative Poisson's ratio in plane elasticity. In Encyclopedia of Continuum Mechanics, eds. H. Altenbach and A. Ochsner (Berlin: Springer). 1800-1806.

[8] Wang, Y., Ko, T. & Ren, X. (2020). Effective mechanical responses of a class of 2D chiral materials. Phys. Status Solidi (b), 257(10) 2000277.

[9] Lakes, R. S., Lee, T., Bersie, A. & Wang, Y. C. (2001). Extreme damping in composite materials with negative-stiffness inclusions. Nature, 410(6828), 565-567.

[10] Jaglinski, T., Kochmann, D., Stone, D. & Lakes, R. S. (2007). Composite materials with viscoelastic stiffness greater than diamond. Science, 315(5812), 620-622.

[11] Wang, Y. C. & Lakes, R. S. (2004). Stable extremely-high-damping discrete viscoelastic systems due to negative stiffness elements. Applied Physics Letters, 84(22), 4451-4453.

[12] Wang, Y. C. & Lakes, R. S. (2001). Extreme thermal expansion, piezoelectricity, and other coupled field properties in composites with a negative stiffness phase. Journal of Applied Physics, 90(12), 6458-6465.

[13] Wang, Y. C., Ko, C. C. & Chang, K. W. (2015). Anomalous effective viscoelastic, thermoelastic, dielectric and piezoelectric properties of negative-stiffness composites and their stability. Physica Status Solidi (b), 252(7), 1640-1655.

[14] Wang, Y., Ko, C., Chang, K. & Ko, T. (2021). Negative-stiffness composite systems and their coupled-field properties. Continuum Mechanics and Thermodynamics, 33(4), 1857-1872.